



A Journal of



## Accepted Article

**Title:** Kinetic-Mechanistic and Solid State Study of the Iodomethane Oxidative Addition to and Migratory Insertion in [Rhodium(S,O-BdiPT or N,O-ox)(CO)(PR<sub>1</sub>R<sub>2</sub>R<sub>3</sub>)] Complexes

**Authors:** Andreas ROODT, Stefan Warsink, Stefanus Otto, Rickert P.D. Kotze, Inus J.M. Janse van Rensburg, Johan Andries Venter, and Ebrahiem Botha

This manuscript has been accepted after peer review and appears as an Accepted Article online prior to editing, proofing, and formal publication of the final Version of Record (VoR). This work is currently citable by using the Digital Object Identifier (DOI) given below. The VoR will be published online in Early View as soon as possible and may be different to this Accepted Article as a result of editing. Readers should obtain the VoR from the journal website shown below when it is published to ensure accuracy of information. The authors are responsible for the content of this Accepted Article.

**To be cited as:** *Eur. J. Inorg. Chem.* 10.1002/ejic.201800293

**Link to VoR:** <http://dx.doi.org/10.1002/ejic.201800293>

WILEY-VCH

# Kinetic-Mechanistic and Solid State Study of the Iodomethane Oxidative Addition to and Migratory Insertion in [Rhodium(*S,O-BdiPT* or *N,O-ox*)(CO)(PR<sup>1</sup>R<sup>2</sup>R<sup>3</sup>)] Complexes

Stefan Warsink<sup>a</sup>, P. D. Riekert Kotze<sup>a,b</sup>, J.M. (Inus) Janse van Rensburg<sup>a,c</sup>, Johan A. Venter<sup>a,\*</sup>, Stefanus Otto<sup>a,b</sup>, Ebrahiem Botha<sup>a</sup>, Andreas Roodt<sup>a,\*</sup>

<sup>a</sup> Department of Chemistry, University of the Free State, PO Box 339, Bloemfontein 9300, South Africa;

<sup>b</sup> Sasol Technology, R&D Division, 1 Klasie Havenga Street, Sasolburg 1948, South Africa.

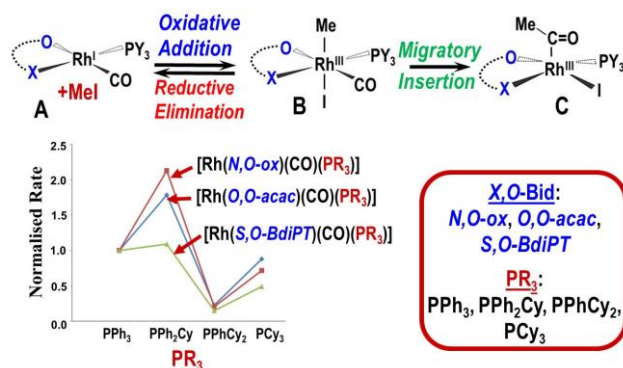
<sup>c</sup> Current address: Wildlife Pharmaceuticals (PTY) Ltd, 38 Wilken Street, Rocky Drift, White River 1240, South Africa.

## Keywords

Rhodium. Oxidative addition. Mechanism. Kinetics. Crystal structures. Bidentate thiourea. Oxine.

## Graphic Contents Illustration

Synthesis and structural characterization of [Rh(*X,O-Bid*)(CO)(PR<sup>1</sup>R<sup>2</sup>R<sup>3</sup>)] (*X,O-Bid*H: *N*-benzoyl-*N',N'*-(diphenyl)thiourea= *S,O-BdiPTH*; *N,O-ox*H = 8-hydroxyquinoline) rhodium(I) carbonyl complexes (**A**) bearing different PR<sub>3</sub> ligands are described, with focus on relative reactivities of iodomethane oxidative addition reactions via intermediate Rh<sup>III</sup>-alkyl complexes (**B**) to Rh<sup>III</sup>-acyl species (**C**).



## Abstract

Rhodium(I) carbonyl complexes containing bidentate *X,O*-Bid (*S,O*-*BdiPT* or *N,O*-*ox*; *N*-benzoyl-*N',N'*-(diphenyl)thiourea = *S,O*-*BdiPTH*; *N,O*-*oxH* = 8-hydroxyquinoline) ligands of the form [Rh(*X,O*-Bid)(CO)(PR<sup>1</sup>R<sup>2</sup>R<sup>3</sup>)] (R<sup>1</sup>, R<sup>2</sup>, R<sup>3</sup> = Ph or Cy) bearing different phosphine ligands, were investigated, the structural characterization of four example complexes is described and an extensive spectroscopic kinetic-mechanistic study of the iodomethane oxidative addition thereto is discussed. Reaction with iodomethane led to Rh<sup>III</sup>-acyl species as secondary (final) products, whereas the primary Rh<sup>III</sup>-alkyl complexes, although rapidly formed, were only observed as intermediates, in small quantities for *S,O*-*BdiPT* (large S-Rh-O bite angle of 90-91°) but in significant amounts for *N,O*-*ox* complexes (less steric with a smaller N-Rh-O bite angle of 79-80°). Overall, almost an order-of-magnitude difference in rate constants was observed for the *S,O*-*BdiPT* complexes, with the PPh<sub>2</sub>Cy- and PPhCy<sub>2</sub>-bearing complexes showing the largest variation. In both the *S,O*-*BdiPT* and *N,O*-*ox* ligand systems an associative activation is inferred from the large negative  $\Delta S^\ddagger$  values. The relative reactivity of Rh<sup>I</sup>-*X,O*-Bid complexes, where X = O, S or N, follows a surprising similar reactivity relationship when stepwise varying the PPh<sub>3</sub>, PPh<sub>2</sub>Cy, PPhCy<sub>2</sub> and PCy<sub>3</sub> tertiary phosphine ligands, suggesting a systematic behavior by the PR<sub>3</sub> ligands, independent of the *X,O*-Bid ligand at the Rh(I) metal centre.

## Introduction

Oxidative addition reactions on metal complexes represent key steps in many catalytic processes, including the carbonylation of methanol. It has been argued that it is the rate-determining step in the catalytic cycles of some of these processes, and therefore any influence on this step can determine the course of the complete catalytic cycle. Due to the vital role of this reaction, a significant amount of research has thus been focused on oxidative addition reactions in order to understand its kinetic properties and responses to external and internal influences.<sup>1</sup>

Iodomethane oxidative addition on rhodium carbonyl complexes is important in industrial production plants utilising the Monsanto and Cativa processes<sup>2</sup> and has been studied intensively with a variety of mono- and bidentate ligands.<sup>3</sup> In general, it was discovered that changing the type of ligand or altering the stereo-electronic properties of the ligand result in significant changes in the outcome of the catalytic process. The carbonyl ligand is essential to allow the formation of acyl adducts via migratory insertion into the metal alkyl bonds formed during the oxidative addition of alkyl iodides. In the Monsanto

process the metal carbonyl species is  $[\text{Rh}^{\text{I}}(\text{I})_2(\text{CO})_2]^-$ , which is relatively unstable. Rhodium carbonyl species containing phosphine ligands and/or bidentate ligands are generally found to be more stable, although some interesting recent metallophilic interactions have been described in Rh(I) dicarbonyl complexes.<sup>4</sup> Furthermore, by tuning the stereo-electronic properties of these ligands, the carbonylation process is directed towards different outcomes. For example, other products might arise if hydrogenation precedes the reductive elimination.

In the case where bidentate ligands containing a sulfur donor atom, in particular thioacetylacetone, were used, the oxidative addition of iodomethane primarily led to the formation of  $\text{Rh}^{\text{III}}$ -acyl complexes.<sup>5,6,7</sup> As we were interested in the synthesis and isolation of  $\text{Rh}^{\text{III}}$ -acyl complexes in our studies towards the reductive carbonylation of methanol, we pursued the synthesis and application of  $[\text{Rh}(\text{S},\text{O}-\text{BdiPT})(\text{CO})(\text{PR}^1\text{R}^2\text{R}^3)]$  species, because in conjunction with the fact that sulfur-containing bidentate ligands lead to  $\text{Rh}^{\text{III}}$ -acyl formation, little data is available on rhodium complexes bearing *S,O*-bidentate ligands.<sup>3,7</sup>

However, we further opted to introduce a smaller bite angle *N,O-ox* ligand 8-hydroxyquinoline (oxine) to compare the behavior with the said *S,O-BdiPT* thiourea based chelates therewith and evaluate/ quantify the origin of the behavior as a function of donor atom (S vs.N vs.O) since it is known that  $\text{Rh}^{\text{I}}$ -oxinato complexes yielded alkyl species as products.<sup>8</sup>

We are in particular aware that much current 'mechanistic research' often involves purely the analysis of reactants and products, while the time-resolved details are much less studied. Thus, here we emphasize the importance of detailed structure-*reactivity* studies in basic catalytic processes to ensure that the complete picture is considered. Moreover, we illustrate here the fact that two clear consecutive reactions as observed, should be carefully considered taking the broader system into account, before simplified to 'one' reaction.

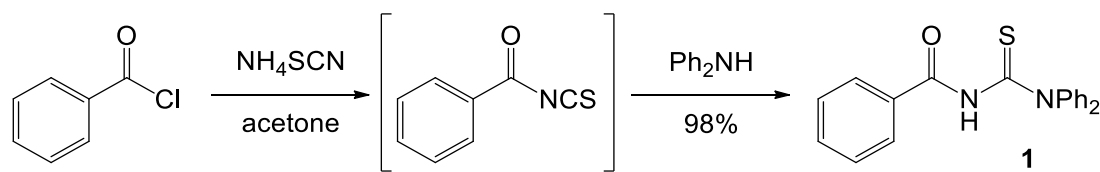
Thus, in this report, the synthesis of selected  $[\text{Rh}(\text{N},\text{O-ox})(\text{CO})(\text{PR}^1\text{R}^2\text{R}^3)]$  and  $[\text{Rh}(\text{S},\text{O}-\text{BdiPT})(\text{CO})(\text{PR}^1\text{R}^2\text{R}^3)]$  complexes ( $\text{PR}^1\text{R}^2\text{R}^3 = \text{PPh}_3, \text{PPh}_2\text{Cy}, \text{PPhCy}_2, \text{PCy}_3$ ; *S,O-BdiPTH*= *N*-benzoyl-*N',N'*-(diphenyl)thiourea and *N,O-oxH*=oxine; 8-hydroxyquinoline) is described to carefully evaluate the effects resulting from the introduction of the *N,O*-bidentate and *S,O*-bidentate ligand systems. In particular, the latter (*S,O-BdiPT*) contains a softer donor atom combination but a larger bite angle (six membered chelate ring) while in the former (*N,O-ox*) a smaller bidentate bite angle (five membered chelate) is introduced; thus varied steric crowding at the Rh(I) centre. Additionally, the kinetic and thermodynamic aspects of the oxidative addition of iodomethane are discussed in relation with the previously

reported *O,O*-acetylacetonato (acac) complexes.<sup>7</sup> Four crystal structures of the starting complexes are reported and are carefully correlated with the steric and electronic properties of the said complexes.

## Results and discussion

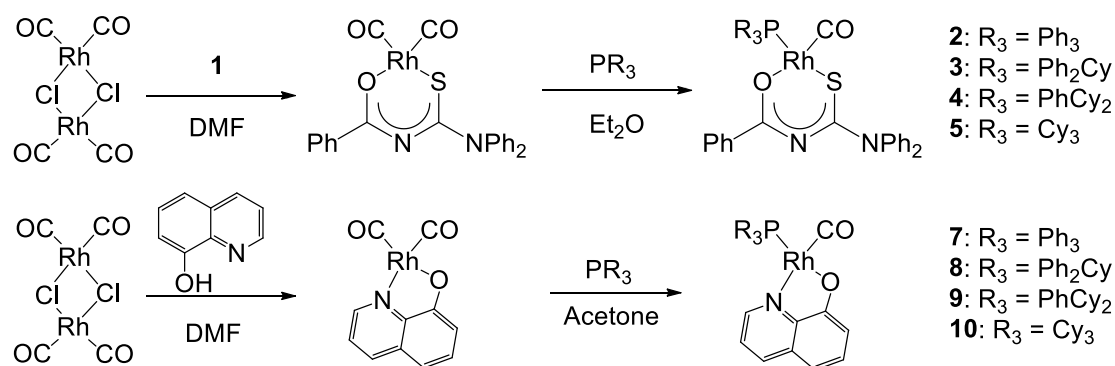
**Ligand and complex synthesis.** The ligand *N*-benzoyl-*N'*,*N'*-(diphenyl)thiourea (*S,O*-*BdiPT*)H was synthesized in two steps from benzoyl chloride (Scheme 1).<sup>9</sup> First, the isothiocyanate was formed, followed by addition of diphenyl amine, which gave the product **1** in an overall yield of 98%.

The <sup>1</sup>H NMR of **1** features a signal at 11.19 ppm, which corresponds with the acidic proton on the thiourea-nitrogen. In the <sup>13</sup>C NMR, the thiourea- and amide-signals are observed at 184.5 and 167.3 ppm, respectively.



**Scheme 1.** Synthesis of *N*-benzoyl-*N'*,*N'*-(diphenyl)thiourea (*S,O*-*BdiPT*)H (**1**).

In order to obtain complexes **2** - **5**, ligand **1** was added to a DMF solution of tetracarbonyl-dichlorido-dirhodium(I),<sup>10</sup> after which the mononuclear dicarbonyl thioureato complex was precipitated with ice water. This complex was only stable in the solid state for a short time and was consequently employed in the next step without detailed characterization. The infrared doublet, characteristic of the symmetric and asymmetric stretching bands of the reactant were clearly observed on ATR. The solid obtained was taken up in diethyl ether, after which the tertiary phosphine ligand was added to the reaction mixture. The desired rhodium(I)-complex precipitated from the solution, from which it was isolated by filtration in yields of 60 - 65% over two steps (Scheme 2). Similarly, complexes **7-10** were obtained as described above for the *S,O*-*BdiPT* complexes by reacting stoichiometric amounts of 8-hydroxyquinoline with tetracarbonyl-dichlorido-dirhodium(I) in DMF as solvent, whereafter the title compound was obtained by adding PPh<sub>3</sub>, PPh<sub>2</sub>Cy, PPhCy<sub>2</sub>, and PCy<sub>3</sub> in acetone. Through slow evaporation of the solvent, crystals were obtained. [Rh(*N,O-ox*)(CO)(PPh<sub>3</sub>)] (**7**) and [Rh(*N,O-ox*)(CO)(PCyPh<sub>2</sub>)] (**8**) were prepared as already reported previously.<sup>11</sup>



**Scheme 2.** Synthesis of  $Rh^I$ -carbonyl complexes bearing (i) different monodentate tertiary phosphine and (ii) different *S,O-BdiPT* [*N*-benzoyl-*N'*,*N'*-(diphenyl)thiourea (*S,O-BdiPT*)H] or *N,O-ox* (8-hydroxyquinoline; oxine) ligands.

All complexes could be well characterized by infrared and NMR, of which characteristic spectroscopic details are presented in Table 1. The disappearance of the signal for the thiourea hydrogen atom on ligand **1** in the  $^1H$  NMR spectrum upon coordination is indicative of the formation of the monoanionic ligand.<sup>7</sup>

As shown in Table 1, all the  $[Rh(S,O-BdiPT)(CO)(PR^1R^2R^3)]$  complexes ( $PR^1R^2R^3 = PPh_3, PPh_2Cy, PPhCy_2,$  and  $PCy_3$ ) show characteristic signals in the  $^{31}P$  NMR for the phosphorus ligands between 38 and 50 ppm. Only one doublet is observed for each compound, indicating the formation of only one isomer, which is expected to have the phosphine and the sulfur-donor in mutual *trans*-positions. Moreover, a single carbonyl vibration was observed in the IR spectrum between 1960 and 1980  $cm^{-1}$  for each, corroborating the fact that only one isomer is present after the reaction. A high field shift is observed in the  $^{31}P$  NMR when going from complex **2** to complex **5**, i.e. towards more electron donating phosphine ligands. The same trend is observed in the  $^{13}C$  NMR signals of the thioureato-carbon atom and the carbonyl ligand. These observations are commensurate with the higher electron density imparted on the rhodium by the phosphine ligand. The first-order rhodium-phosphorus coupling ( $J_{Rh-P}$ ) and the CO-stretching vibration of the carbonyl ligand decrease from **2** to **5** as expected for this ligand series. In the carbonyl ligand, this is caused by a reduced C-O bond order, due to increased  $\pi$ -back bonding to accommodate the higher electron density on the rhodium metal centre.

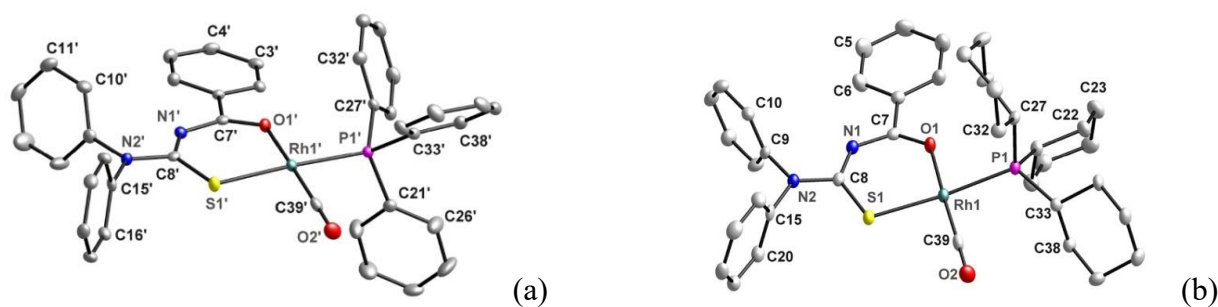
Similar behavior with respect to the IR and  $^{31}\text{P}$  NMR spectroscopic data is observed for the corresponding  $[\text{Rh}(N,O\text{-ox})(\text{CO})(\text{PR}^1\text{R}^2\text{R}^3)]$  complexes (**7-10**), see Table 1.

**Table 1.** Summary of spectroscopic data (solution and solid state) for **2-5**, **7-10**.

	$\text{PR}_3$	<b>2</b> <sup>a</sup>	<b>3</b> <sup>a</sup>	<b>4</b> <sup>a</sup>	<b>5</b> <sup>a</sup>	<b>7</b> <sup>b</sup>	<b>8</b> <sup>b</sup>	<b>9</b> <sup>b</sup>	<b>10</b> <sup>b</sup>
IR	$\nu_{\text{CO}}(\text{cm}^{-1})$	1979	1972	1969	1963	1965	1968	1952	1946
	$\nu_{\text{CO}}(\text{cm}^{-1})$	1963 <sup>c</sup>	1966 <sup>c</sup>	1961 <sup>d</sup>	1952 <sup>c</sup>	1959 <sup>d</sup>	1959 <sup>d</sup>	1952 <sup>d</sup>	1946 <sup>d</sup>
$^{31}\text{P}$ NMR	$\delta(\text{ppm})$	38.2	49.5	49.5	49.9	41.2	52.8	53.6	54.8
	$J_{\text{Rh-P}}/\text{Hz}$	152	149	149	146	164	163	161	156

<sup>a</sup>  $\text{CH}_2\text{Cl}_2$ , unless otherwise stated; <sup>b</sup> Acetone, unless otherwise stated; <sup>c</sup> Neat samples, ATR; <sup>d</sup> IR KBr

**X-ray crystallography.** Detailed structural information of these complexes was obtained from crystallographic analyses. Single crystals were obtained by slow evaporation of a dichloromethane/acetone solution of complexes **2**, **3**, **5** and **10**, yielding the subsequent molecular structures (Figure 1). Despite our best efforts, no crystals suitable for X-ray analysis could be obtained for complexes **4** and **9**. Complexes **7** and **8** are referenced<sup>11</sup> from literature for completeness. The basic crystallographic parameters and data collection details are given in the Supplementary Information. All four complexes crystallized in the monoclinic crystal system, with **2**, **3** and **5** in space group  $P2_1/c$ , and **10** in  $C2/c$ . In Table 2 a comparison between selected bond lengths and angles of the complexes is presented.



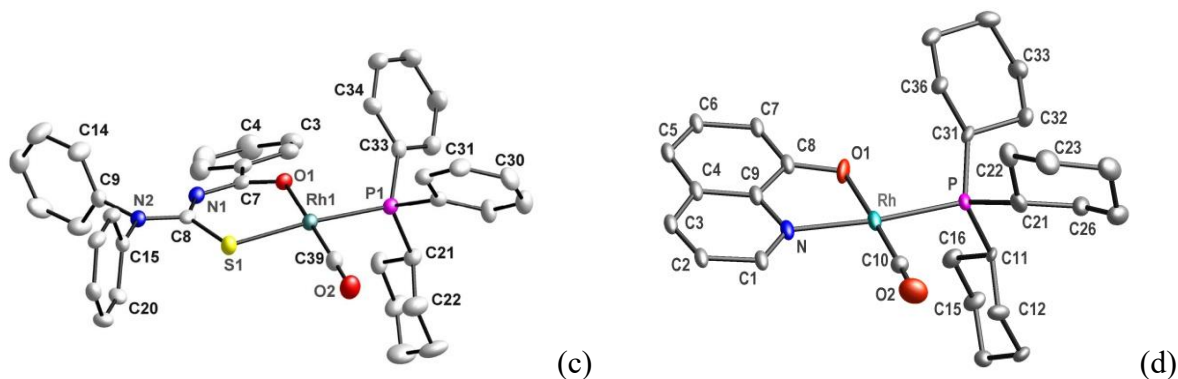


**Figure 1.** Displacement ellipsoid plots of (a) **2'** (only 1 molecule displayed; other one very similar, (b) **3**, (c) **5**; (30% probability level) and (d) **10** (50% probability level). H-atoms are omitted for the sake of clarity and only relevant atoms are labeled.

Complex **2** crystallized with two slightly different independent molecules (relative variation in bonds and angles indicated in Table 2) in the asymmetric unit. Both are very similar in terms of their basic bond lengths and angles, with the main difference being the rotation of the phenyl rings, both on the phosphine and the *S,O-BdiPT* ligands.

All complexes show a slightly distorted square planar geometry, amongst other due to the larger than 91° bite angle of the *S,O-BdiPT* ligand (S-Rh-O1). The bidentate ligand shows delocalization of electron density, borne out by the bond lengths that lie between those of single and double bonds (for full crystallographic data, see Supporting Information). To accommodate the square planar geometry, the *S,O-BdiPT* ligand shows a small rotation with respect to its backbone as manifested by the torsion angle. The different phosphine ligands have the expected effect on bond lengths, with the more electron-donating but bulky ligands having a *longer* bond to rhodium (Rh-P) and conversely lengthening the bond to the trans-ligand (Rh-S) as well. The phosphine ligands also influence the carbonyl ligands, although the shortening of the Rh-C39 bond length and the elongation of the C39-O2 bond length with more basic phosphines is not significant. It is noted that the carbonyl ligand shows a slight distortion from linearity in its coordination in the solid state, although the cause for this is unclear and might be due to packing effects.

The Rh-P bond lengths (*trans* to the *S*-atom) of the *S,O-Bid* ligands in this study are ca 2.27-2.30 Å and significantly longer when compared to the Ph-P bonds (*trans* to *O*-atom) of ca. 2.23-2.24 Å, *i.e.*, with

that of the acac ligand (*O,O*-Bid ligand) in a previous investigation, clearly showing an increase in Rh-P bond lengths, in agreement with the larger trans influence of the *S*-donor ligand. The increase in bond lengths is also manifested in the  $^1J(^{31}\text{P}-^{103}\text{Rh})$  coupling constants shown in Table 1 (around 155 Hz for the *S,O*-Bid ligands, compared to ca. 170 Hz for the *O,O*-Bid ligands such as acac).<sup>7</sup>

**Table 2.** Selected bond lengths (Å) and angles (°) for complexes **2**, **3**, **5**, **8** and **10**.

Bond/ Angle	[Rh( <i>S,O</i> - <i>BdiPT</i> )(CO)(PR <sub>3</sub> )]				Bond/ Angle	[Rh( <i>N,O</i> - <i>ox</i> )(CO)(PR <sub>3</sub> )]	
	2	2' <sup>a</sup>	3	5		<b>8</b> <sup>11</sup>	10
Rh-S	2.304(1)	2.312(1)	2.312(1)	2.329(1)	Rh-N	2.128(2)	2.091(4)
Rh-O1	2.039(2)	2.037(2)	2.037(3)	2.057(3)	Rh-O1	2.060(2)	2.036(4)
Rh-P	2.291(1)	2.278(1)	2.287(1)	2.302(1)	Rh-P	2.2798(8)	2.2557(15)
Rh-C39	1.791(3)	1.804(3)	1.798(5)	1.788(5)	Rh-C10	1.803(3)	1.1817(6)
C39-O2	1.154(4)	1.153(4)	1.155(5)	1.157(6)	C8-O1	1.328(3)	1.321(7)
S···O1 (distance)	3.105	3.126	3.110	3.153	N···O	2.676(3)	2.671(5)
S-Rh-O1 (bite)	91.1(1)	91.7(1)	91.1(1)	91.7(1)	O1-Rh-N	79.41(9)	80.65(16)
O1-Rh-P	87.5(7)	89.5(1)	89.5(1)	88.7(1)	P-Rh-O1	93.11(6)	91.14(11)
P-Rh-C39	93.0(1)	88.5(1)	89.0(1)	90.2(2)	C10-Rh-P	88.70(10)	90.89(18)
C39-Rh-S	88.9(1)	90.1(1)	90.1(1)	90.2(2)	N-Rh-C10	99.10(12)	97.3(2)
Rh-C39-O2	175.3(3)	177.6(3)	177.8(4)	178.0(5)	Rh-C10-O2	179.6(3)	176.5(5)

<sup>a</sup> **2'** second molecule in the asymmetric unit

Complex **10** crystallized with eight molecules in the unit cell (*Z*=8) in the monoclinic space group *C2/c*. Figure 1 shows the general numbering scheme of **10** and the most important bond distances and angles are reported in Table 2. The fused ring system of the bidentate ligand is almost planar, with an r.m.s deviation between atoms C1-C9 and N of 0.0139 Å, as further emphasized by the dihedral angle between the two aromatic rings of 1.5(3)°. The distorted square-planar metal coordination polyhedron is illustrated by the bite angle of 80.65(16)° and a C10-Rh-P bond angle of 90.89(18)°. The carbonyl ligand is close to linearity with a Rh-C10-O2 angle of 176.5(5)°. A slight molecular bending is displayed by the dihedral angle of 7.18(10)° which formed between the fused ring system plane and the metal coordination plane. The rhodium metal centre is displaced 0.170(5) Å from the fused ring system plane and 0.0118(5) Å out of the metal coordination plane. By calculating the effective cone angle (θE) 167° and using the actual Rh-P bond distance of 2.256(2) Å, steric demand of the tricyclohexylphosphine in the

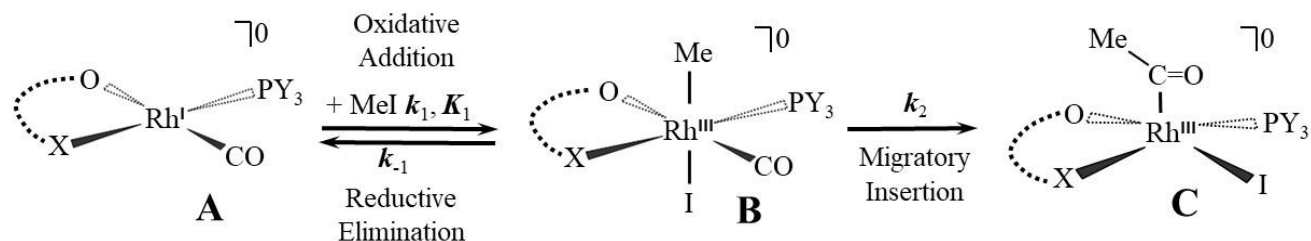
solid state, could be determined.<sup>14,15</sup> The molecular crystal packing is stabilized by a ligand  $\pi$ - $\pi$  stacking and soft contacts between the aryl substituted rings of the phosphorous ligand and the quinoline ligand of the next molecule.

Compound **8** crystallized in the monoclinic space group  $P2_1/n$ , ( $Z=4$ ). Figure 1 contains the general atom numbering used for **8**. The fused ring system of the bidentate ligand is bending slightly, with a r.m.s. deviation from planarity of 0.0214 Å and a dihedral angle of 2.0(1)° between the two aromatic rings of the oxinate ligand, indicating a slight distortion in the ligand backbone. A further distortion is observed between the bidentate  $N,O$ -ox backbone and the metal coordination plane, yielding a dihedral angle of 11.3(1)°. In the five membered chelate ring, the  $N,O$ -ox ligand has a small bite angle of 79.41(9)° and a C10-Rh-P angle of 88.70(10)°, which illustrates the distorted square-planar metal coordination polyhedron. The rhodium atom lies in a general position and is slightly displaced out of the coordination plane by 0.062 (1) Å (r.m.s. displacement of fitted atoms = 0.098 Å). The carbonyl ligand is mostly linear with an Rh-C10-O2 angle of 179.6(3)°. The significant steric demand of the cyclohexyldiphenylphosphine ligand (in the solid state) was determined to be 151°. This was done by calculating the effective cone angle ( $\theta_E$ ) using the actual Rh-P bond distance of 2.2798(8) Å. The most important bond distances and angles are reported in Table 2.

### **Kinetic experiments.**

**[Rh(*S,O*-BdiPT)(CO)(PR<sub>3</sub>)] complexes.** When complex **2** was reacted with iodomethane in dichloromethane under pseudo first-order conditions, *in situ* IR-spectroscopy showed [Fig. 2(a)] that the carbonyl signal of the reactant at 1979 cm<sup>-1</sup> disappeared, while a signal at 1715 cm<sup>-1</sup> appeared virtually simultaneously. The latter signal corresponds to a rhodium(III)-acyl species, indicating that conversion of the Rh<sup>I</sup>-carbonyl complex proceeds to the insertion product. However this proceeds *via* a Rh<sup>III</sup>-alkyl complex, which is only minutely observed by the signal at 2065 cm<sup>-1</sup>. This implies that the rate of conversion to the rhodium(III)-alkyl complex would be difficult if not virtually impossible to analyze and that the major reaction rate involved is the ‘direct’ conversion of **2** to the Rh<sup>III</sup>-acyl complex.

The iodomethane oxidative addition/ reductive elimination, and subsequent migratory carbonyl insertion are illustrated in Scheme 3, which suggests the formation of the intermediate Rh<sup>III</sup>-alkyl species **B** and the subsequent formation of the Rh<sup>III</sup>-acyl species **C**.



**Scheme 3.** Oxidative addition of iodomethane followed by migratory insertion of CO [*X,O*-Bid= *S,O*-*BdiPT* or *N,O*-*ox*).

The change in the IR absorbance values for the different species over the time period in which the reaction was studied, is shown in Figure 2(a). The seemingly ‘direct’ conversion of the starting complex **2** to the Rh<sup>III</sup>-acyl complex is evident by comparing the disappearing and formation rates of the two separate species. Note that the reaction was completed after less than 60 min, yielding a pseudo first-order rate for the disappearance of the starting complex [Rh(*S,O*-*BdiPT*)(CO)(PPh<sub>3</sub>)] (1.84±0.01) × 10<sup>-3</sup> s<sup>-1</sup>, very similar to the rate of formation of the acyl species [Rh(*S,O*-*BdiPT*)(COMe)(I)(PPh<sub>3</sub>)] (2.01±0.02) × 10<sup>-3</sup> s<sup>-1</sup>. The difference between these two values is attributed to baseline drift during the measurement and the small contribution from the formation of the intermediate Rh<sup>III</sup>-alkyl species.

This behavior has been reported previously by several authors, where the oxidative addition of iodomethane to rhodium complexes bearing a bidentate ligand incorporating a sulfur donor atom led primarily to the formation of Rh<sup>III</sup>-acyl complexes.<sup>5,12</sup> Furthermore, in these publications it was also shown that only a small amount of the Rh<sup>III</sup>-alkyl species was observed. Recent work showed again that by changing the bidentate ligand from an *S,O*-*BdiPT* to an *O,O*-*Bid* type, the reaction can be influenced to ensure slower acyl-formation compared to the oxidative addition.<sup>13</sup> This was indeed the case for the *N,O*-*ox* ligands, see discussion below.

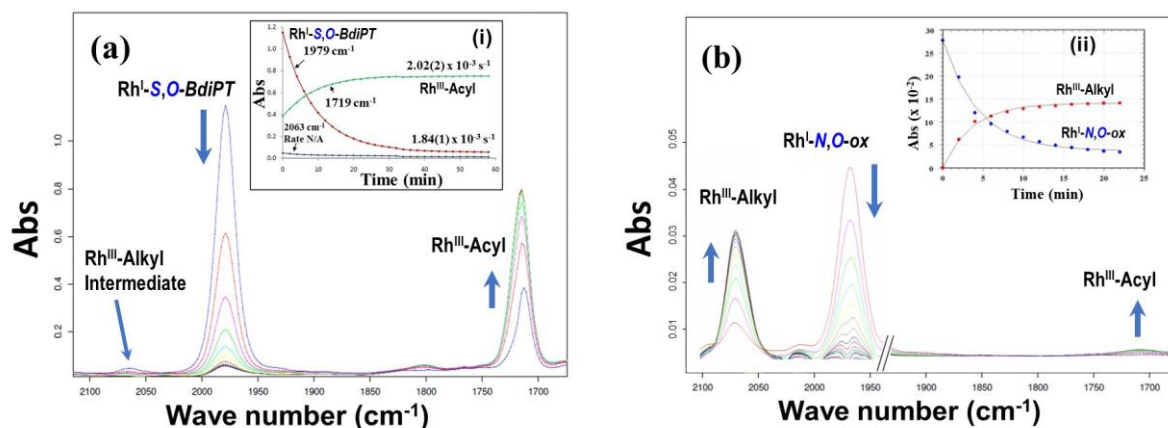


**Figure 2.** Successive IR spectra for the iodomethane oxidative addition to (a)  $[\text{Rh}(\text{S},\text{O}\text{-}\text{BdiPT})(\text{CO})(\text{PPh}_3)]$  (**2**) under pseudo first-order conditions in  $\text{CH}_2\text{Cl}_2$  at  $25^\circ\text{C}$ . Spectra recorded at time intervals of 6 min., with  $[\text{Rh}] = 0.0105\text{ M}$ ,  $[\text{MeI}] = 0.4\text{ M}$ ,  $T = 25^\circ\text{C}$ , total time = 1 hr. Insert (i) illustrates the IR absorbance change vs. time plot; pseudo first-order rate constants indicate that the disappearance of the  $\text{Rh}^{\text{I}}$  (red) is similar to the formation of  $\text{Rh}^{\text{III}}$ -acyl (green) with  $\text{Rh}^{\text{III}}$ -alkyl (blue); (b)  $[\text{Rh}(\text{N},\text{O}\text{-}\text{ox})(\text{CO})(\text{PPh}_3)]$  (**7**), which illustrates the conversion of the  $\text{Rh}^{\text{I}}$  starting complex ( $1965\text{ cm}^{-1}$ ) to the  $\text{Rh}^{\text{III}}$ -alkyl species ( $2057\text{ cm}^{-1}$ ). Scans were recorded at 2 min intervals,  $[\text{Rh}(\text{N},\text{O}\text{-}\text{ox})(\text{CO})(\text{PPh}_3)] = 1.1 \times 10^{-3}\text{ M}$  and  $[\text{MeI}] = 9.82 \times 10^{-2}\text{ M}$ .  $k_{\text{obs}}(\text{Rh}^{\text{I}}) = 3.8(2) \times 10^{-3}\text{ s}^{-1}$  and  $k_{\text{obs}}(\text{Rh}^{\text{III}}) = 4.0(2) \times 10^{-3}\text{ s}^{-1}$ . Insert (ii) illustrates of the carbonyl peak change over time with the iodomethane oxidative addition to the complex  $[\text{Rh}(\text{N},\text{O}\text{-}\text{ox})(\text{CO})(\text{PPh}_3)]$ , in  $\text{CH}_2\text{Cl}_2$  at  $25^\circ\text{C}$ . Decrease in  $\text{Rh}^{\text{I}}(\text{N},\text{O}\text{-}\text{ox})$  (blue); formation of  $\text{Rh}^{\text{III}}$ -alkyl (red).

When an equilibrium is assumed for the first step in Scheme 3 (oxidative addition),<sup>14</sup> with reductive elimination being the reverse reaction, it follows naturally from the observed behavior that the equilibrium when lying to the left (small  $K_1 = k_1/k_{-1}$ ) and the acyl-formation ( $k_2$ ) in combination with the rapid pre-equilibrium of the formation of the  $\text{Rh}^{\text{III}}$ -alkyl species essentially dictates the turnover rate as defined in Eq. 1 (Scheme 3). This was the case for the *S,O-BdiPT* complexes.

The observed pseudo first-order formation rate constant,  $k_{\text{obs}}$  of the  $\text{Rh}^{\text{III}}$ -acyl species, is thus defined in Eq. 1.<sup>14</sup>

$$k_{\text{obs}} = K_1 k_2 [\text{MeI}] / (1 + K_1 [\text{MeI}]) + k_{-2} \cong k_2' [\text{MeI}] \quad (1)$$

In Eq. 1,  $k_2' = K_1k_2$  when  $K_1 \ll 1$ , and the reverse reaction of the migratory insertion as defined by  $k_{-2}$  is negligible (zero intercept in Fig. 4).

For complexes **4** and **5** similar behavior was observed, with the ‘direct’ conversion of the starting complex to the Rh<sup>III</sup>-acyl complex as most striking feature. However, in the reaction of complex **3** with iodomethane, a more significant amount (although still quite low) of the Rh<sup>III</sup>-alkyl intermediate was observed (see Supporting Information). Apparently, the equilibrium of the oxidative addition/reductive elimination does not lie as far to the left as with the other complexes. Additionally, two signals attributed to Rh<sup>III</sup>-alkyl species were observed (see Supplementary Information). This indicates that two isomers are probably formed, corresponding to potentially *cis*- and *trans*-addition of iodomethane.

Preliminary kinetics of the formation of the Rh<sup>III</sup>-alkyl intermediate was attempted by stopped-flow measurements with UV/vis detection, but the absorbance changes were not significant enough to allow for accurate interpretation. However, in spite of the fact that these first reactions could not be studied with accuracy, they were clearly and distinctly different from the mixing reaction in the stopped-flow, of which the conversions were in agreement with the amounts identified on the Infrared Spectroscopy stack-plots (i.e., Fig. 2, as well as Supporting Information). Moreover, these reactions were a few seconds and clearly much faster than the formation of the Rh<sup>III</sup>-acyl species (several minutes). They are also more pronounced at higher [MeI] indicating they are equilibrium reactions. The conclusion is thus that formation of the Rh<sup>III</sup>-alkyl species is fast as shown in Scheme 3, and that Eq. 1 adequately describes the kinetics.

The conversion of the Rh<sup>I</sup>- to the Rh<sup>III</sup>-form could also be observed in <sup>31</sup>P NMR for all four complexes (see Fig. 3 and Supporting Information), and agrees very well with that observed from the IR data. Kinetic and spectroscopic data (where applicable) obtained from Eq. 1 for the *S,O-BdiPT* complexes as described above, are summarized in Table 3 together with the Bronsted  $pK_a$  of the free phosphine, as well as the enthalpies and entropies of activation (*vide infra*).

**[Rh(*N,O-ox*)(CO)(PR<sub>3</sub>)] complexes.** However, interestingly in the case of the *N,O-ox* ligand complexes, a different scenario is observed from the time resolved IR spectroscopic results, see Fig. 2(b). The significant amount of Rh<sup>III</sup>-alkyl intermediate is clear [ $\nu(\text{CO})=2057 \text{ cm}^{-1}$ ]. This behavior is confirmed by the time resolved <sup>31</sup>P NMR spectra, see Fig. 3(b). Clearly, the Rh<sup>III</sup>-alkyl intermediate species

in this case is prominently visible on the  $^{31}\text{P}$  spectra (as was the case on the IR data; see Fig. 3(b)), with the formation of the  $\text{Rh}^{\text{III}}$ -acyl species (**C** in Scheme 3) being formed thereafter.

In this case, the oxidative addition of iodomethane is simply described by Eq. 2, which is obtained for the formation of **B** Scheme 3 from **A** via a simple equilibrium as shown previously.<sup>13,14</sup> However, in this case this equilibrium clearly lies significantly towards **B**.

$$k_{\text{obs}} = k_1[\text{MeI}] + k_{-1} \quad (2)$$

Thus, Eq. 2 was used to obtain the rates of oxidative addition for the *N,O-ox* complexes and are summarized in Table 3.

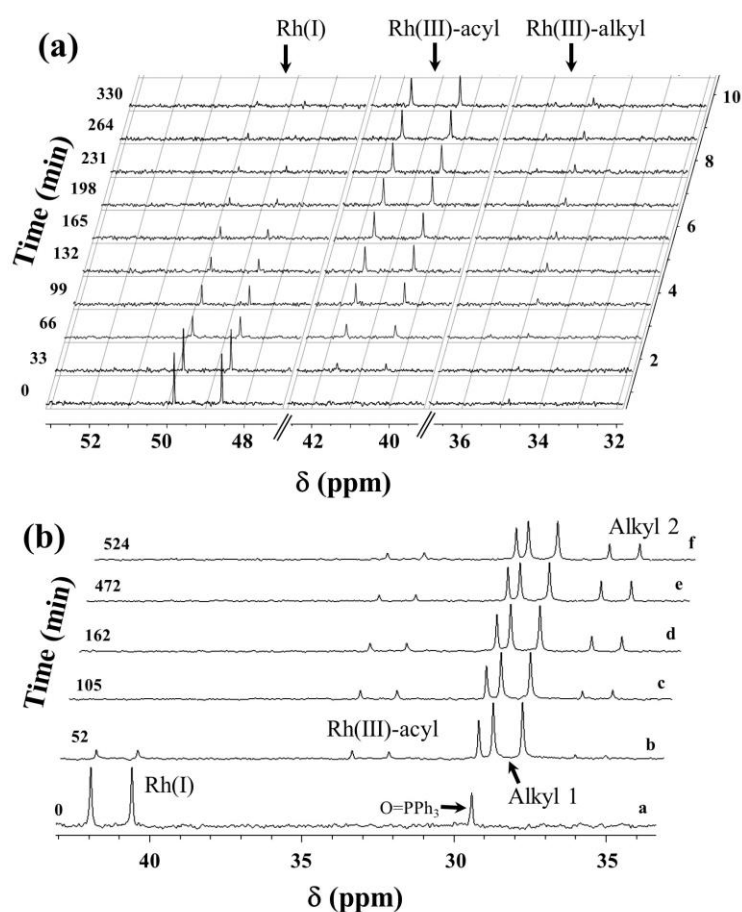


**Figure 3.** (a) Observed  $^{31}\text{P}\{^1\text{H}\}$  NMR spectra of the iodomethane oxidative addition to  $[\text{Rh}(\text{S},\text{O}-\text{BdiPT})(\text{CO})(\text{PPhCy}_2)]$  in  $\text{CD}_2\text{Cl}_2$ . Time intervals in minutes indicated on the left of spectra.  $[\text{Rh}] = 0.081$  M,  $[\text{MeI}] = 0.4$  M,  $T = 25$  °C; total time = 8.8 hrs.  $^{31}\text{P}$  NMR were recorded with the default setting of  $^1\text{H}$  decoupling using the WALTZ16 method, typical 128 scans, a sweep width of 400.5 ppm (48661.8 Hz), delay time (D1) of 2 sec. and 64 K Points. (b) Observed  $^{31}\text{P}\{^1\text{H}\}$  NMR spectra of the  $[\text{Rh}(\text{N},\text{O}-$

*ox*)(CO)(PPh<sub>3</sub>)] complex undergoing iodomethane oxidative addition to form alkyl intermediate(s) [Rh(*N,O-ox*)(CH<sub>3</sub>)(I)(CO)(PPh<sub>3</sub>)] and migratory insertion to form a small amount of the Rh<sup>III</sup>-acyl product, in acetone at 25°C. a) [Rh] = 1.44 × 10<sup>-2</sup> M. b) [Rh] = 1.34 × 10<sup>-1</sup> M, [MeI] = 1.05 × 10<sup>-1</sup> M. c) [Rh] = 1.26 × 10<sup>-1</sup> M, [MeI] = 2.04 × 10<sup>-1</sup> M. d) [Rh] = 1.06 × 10<sup>-1</sup> M, [MeI] = 4.24 × 10<sup>-1</sup> M. e-f) [Rh] = 7.71 × 10<sup>-2</sup> M, [MeI] = 7.52 × 10<sup>-1</sup> M.

Interestingly Fig. 3(b) shows a *second* alkyl species (labeled Alkyl 2) to form later [only some 20% conversion compared to Alkyl 1 (via/ concurrent with acyl species) to Alkyl 2 after >10h] in the total reaction. In contrast Alkyl 1 (monitored in the kinetic study), formed *completely* in only some 30 min. with only small amounts of Rh<sup>III</sup>-acyl being present, see Fig. 2(b) and in particular, Fig. 3(b), spectrum (b). Alkyl 2 is assumed to be the trans isomer [Me vs. I coordination], since the cis isomer is formed first in less steric demanding bidentate ligand systems.<sup>3,8</sup> Thus, the kinetics and dynamics of Alkyl 2, which is formed more than one order-of-magnitude slower than Alkyl 1, was considered beyond the scope of the current study and is therefore not considered further herein.

An important observation to be made from Table 3 is that the spectral data for complexes **2** – **5** that are used to gauge electron-density on the metal center are *not* all reflected in the observed reaction rates. On the basis of the phosphine basicity, it is expected that the rates of oxidative addition would increase when going from complex **2** to complex **5**.<sup>15</sup> However, no such trend is observed in the reaction rates. It appears that the steric bulk of the phosphine ligand beyond a certain point has a significant influence, as well as its basicity. Only a net reaction is observed, which represents a compound observed rate constant as indicated by Eq. 1. This is best illustrated when the reaction rate observed in IR is plotted with respect to the iodomethane concentration, with the solid lines representing the least-squares fit of the data (Fig. 4(a)). An eight times de-activation of specifically complex **4** compared to complex **3** was observed, with complexes **2** and **5** being intermediate.<sup>3,14</sup>

Surprisingly, a very similar trend was observed within the [Rh(*N,O-ox*)(CO)(PR<sup>1</sup>R<sup>2</sup>R<sup>3</sup>)] complexes (**7**–**10**), although a different reaction [direct iodomethane oxidative addition; Fig. 2(b) and 3(b)] compared to the [Rh(*S,O-BdiPT*)(CO)(PR<sup>1</sup>R<sup>2</sup>R<sup>3</sup>)] complexes [overall formation of Rh<sup>III</sup>-acyl species, see Fig. 4(b)]. The *N,O-ox* complexes were approximately one order-of-magnitude progressively faster than the corresponding *S,O-BdiPT* complexes. This will be highlighted further later in the Discussion.

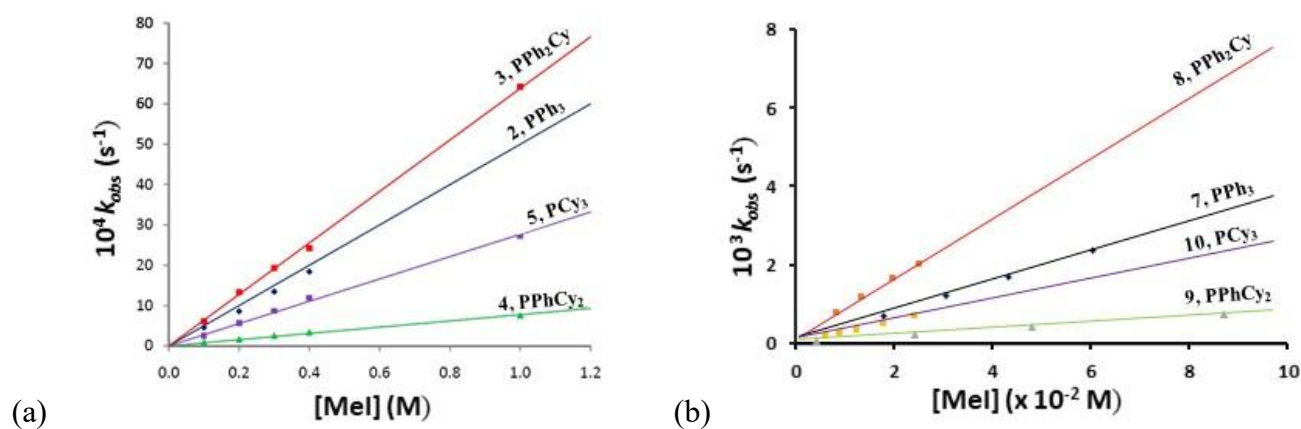


**Figure 4.** Effect of phosphine ligands on the observed rate constants  $k_{\text{obs}}$  vs.  $[\text{MeI}]$  for oxidative addition to (a) Rhodium(I)-*S,O-BdiPT* complex **2** - **5**,  $[\text{Rh}] = 0.010$  M in  $\text{CH}_2\text{Cl}_2$  at  $25^\circ\text{C}$ ; (b) rhodium(I)-*N,O-ox* for the formation of  $[\text{Rh}(\text{N},\text{O-ox})(\text{CH}_3)(\text{I})(\text{CO})(\text{PR}_3)]$  for **7-10**, in acetone at  $25^\circ\text{C}$ .  $[\text{Rh}(\text{N},\text{O-ox})(\text{CO})(\text{PPh}_3)] = 2.394 \times 10^{-4}$  M,  $[\text{Rh}(\text{N},\text{O-ox})(\text{CO})(\text{PPh}_2\text{Cy})] = 2.119 \times 10^{-4}$  M,  $[\text{Rh}(\text{N},\text{O-ox})(\text{CO})(\text{PPhCy}_2)] = 2.230 \times 10^{-4}$  M,  $[\text{Rh}(\text{N},\text{O-ox})(\text{CO})(\text{PCy}_3)] = 2.276 \times 10^{-4}$  M,  $\lambda = 380$  nm.

**Table 3.** Kinetic, spectroscopic and thermodynamic data for the iodomethane oxidative addition/ migratory insertion at  $25^\circ\text{C}$  to **2** - **5** to  $[\text{Rh}(\text{S},\text{O-BdiPT})(\text{CO})(\text{PR}_3)]$  in  $\text{CH}_2\text{Cl}_2$ ; and **7** - **10**  $[\text{Rh}(\text{N},\text{O-ox})(\text{CO})(\text{PR}_3)]$  ( $\text{PR}_3 = \text{PPh}_3, \text{PPh}_2\text{Cy}, \text{PPhCy}_2, \text{PCy}_3$ ) complexes, in acetone.

Complex	$10^3 k_2^a$ (M <sup>-1</sup> s <sup>-1</sup> )	$10^3 k_1^b$ (M <sup>-1</sup> s <sup>-1</sup> )	$\nu_{\text{CO}}$ (cm <sup>-1</sup> )	$\delta^{31\text{P}}$ (ppm)	$^1J_{\text{Rh-P}}$ (Hz)	Cone angle <sup>c</sup> (°)	$\text{p}K_a^d$ free phosphine	$\Delta H^\ddagger$ (kJ/mol)	$\Delta S^\ddagger$ (J/K.mol)
2	5.1±0.3	-	1979	38.0	152	145	3.28	42±2	-147±7
3	6.4±0.3	-	1972	45.3	149	153	5.87	42±1	-146±3
4	0.82±0.08	-	1969	49.3	149	-	8.46	48±1	-144±4
5	2.8±0.02	-	1963	49.9	146	156	11.3	46±2	-140±6
7	-	39±1	1965	41.2	164	156	3.28	58.9±0.2	-74.1±0.06
8	-	86±2	1968	52.8	163	151	5.87	-	-
9	-	8±1	1952	53.6	161	-	8.46	-	-
10	-	28±1	1946	54.8	156	167	11.3	-	-

<sup>a</sup> Calculated from Fig. 4(a) using Eq. 1; <sup>b</sup> Obtained from least-squares fitting of the data in Fig. 4(b) to Eq. 2; <sup>c</sup> Calculated from solid state data; <sup>d</sup> Obtained from Ref. 16

To enable the calculation of the activation parameters for the overall reaction on complexes **2** - **5**, a temperature study was performed. From the obtained values for  $k_2'$ , an Eyring plot was obtained (Fig. 5), which in turn was used to calculate the activation enthalpy and entropy (Table 3). Similar calculations were performed for **7** (using the  $k_1$  data, see Fig. 4(b); Supporting Information) for which the values are also reported in Table 3.

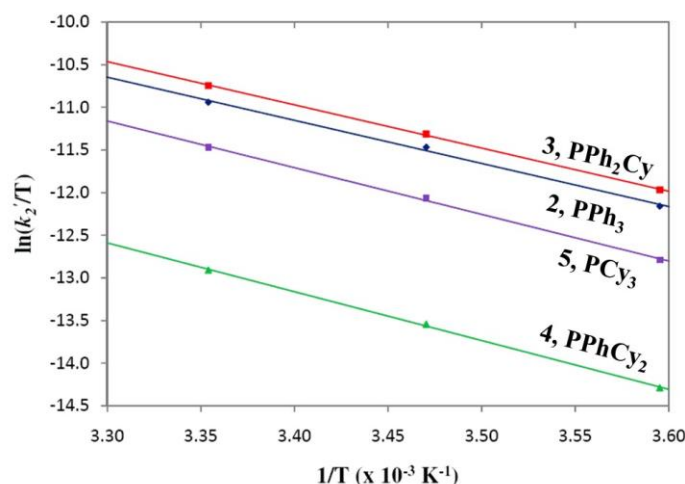


**Figure 5.** Eyring plot for the oxidative addition of iodomethane / methyl migration to  $[\text{Rh}(\text{S},\text{O}-\text{BdiPT})(\text{CO})(\text{PR}_3)]$  (**2** – **5**) in  $\text{CH}_2\text{Cl}_2$ .

The data for the reactions suggest that overall they proceed with large negative entropies of activation, which corresponds to the associative character of the reaction. This holds for both the formation of the octahedral intermediate  $\text{Rh}^{\text{III}}$ -alkyl species, and the subsequent formation of the square-pyramidal  $\text{Rh}^{\text{III}}$ -acyl complex. Furthermore, there is a hint that  $\Delta S^\ddagger$  becomes less negative for complexes bearing more basic phosphine ligands, although it has to be noted that the differences are not significant.

These results suggest that an increase in the electron-donating properties of the phosphine ligand led to an increase in order in the transition state by forming stronger bonds between the metal centre and the entering iodomethane, typical of oxidative addition reactions.<sup>7</sup> The enthalpy of activation is similar for all four complexes, and the values are in a range often found for this reaction, and correlates also directly with the alkyl formation for the beta-diketone complexes with the corresponding four phosphine ligands listed here, as reported previously.<sup>3,14</sup>

Finally, the data in Table 3 for the *S,O-BdiPT* and *N,O-ox* complexes were normalized [considering  $\text{PPh}_3=1$ , and adjusting all the other three rate constants accordingly], and plotted together with that observed for the  $[\text{Rh}(\text{O},\text{O-acac})(\text{CO})(\text{PR}_3)]$  ( $\text{PR}_3 = \text{PPh}_3, \text{PPh}_2\text{Cy}, \text{PPhCy}_2, \text{PCy}_3$ ) from literature,<sup>3</sup> as illustrated in Fig. 6. The relative reactivity of  $\text{Rh}^{\text{I}}\text{-X},\text{O-Bid}$  complexes, where  $\text{X}=\text{O}, \text{S}$  or  $\text{N}$ , follows a surprising similar reactivity relationship when stepwise varying the  $\text{PPh}_3, \text{PPh}_2\text{Cy}, \text{PPhCy}_2$  and  $\text{PCy}_3$  tertiary phosphine ligands. Superficially, it seems as if the differences within the *S,O-BdiPT* series is less significant than that in the *O,O-acac* and the *N,O-ox* series. This might be linked to the fact that in the former the rate constants used ( $k_2'$ ) are combined constants, for which there might be some offset in the other steps making up the constant used. Be that as it may, the similar tendency for all three systems is clear, and indicates the surprising net difference between  $\text{PPh}_2\text{Cy}$  and  $\text{PPhCy}_2$ , wherein the latter clearly has a significant decelerating effect compared to the former.

This will be explored further in future with other model systems, which might prove valuable to exploit the unexpected acceleration/ deceleration by the  $\text{PPh}_2\text{Cy}$  and  $\text{PPhCy}_2$  ligands, respectively.

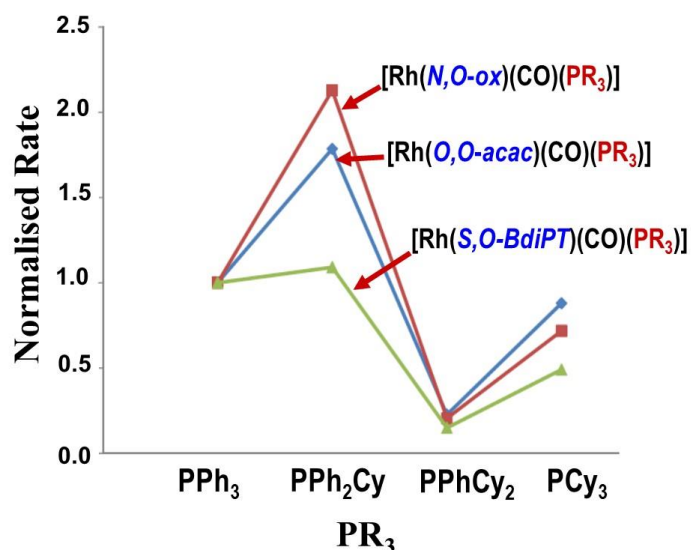


**Figure 6.** Normalized reaction rate constants (relative to the  $\text{PPh}_3, =1$ ) for  $\text{X},\text{O-Bid}$  = oxinato (*N,O-ox*), acetylacetonato (*O,O-acac*) and thioureato (*S,O-BdiPT*);  $\text{PR}_3$  where  $\text{R} = \text{Ph}$  or  $\text{Cy}$  for all complexes at 25 °C.

## Conclusions

The synthesis and characterization of  $[\text{Rh}(S,O\text{-}BdiPT)(\text{CO})(\text{PR}^1\text{R}^2\text{R}^3)]$  and  $[\text{Rh}(N,O\text{-}ox)(\text{CO})(\text{PR}^1\text{R}^2\text{R}^3)]$  ( $\text{PR}^1\text{R}^2\text{R}^3 = \text{PPh}_3, \text{PPh}_2\text{Cy}, \text{PPhCy}_2$  and  $\text{PCy}_3$ ) complexes, including four single crystal structure determinations (compounds **2**, **3**, **5** and **10**) were performed, followed by a detailed mechanistic investigation into the iodomethane oxidative addition thereto.

The oxidative addition to a range of  $[\text{Rh}(S,O\text{-}BdiPT)(\text{CO})(\text{PR}^1\text{R}^2\text{R}^3)]$  complexes ( $S,O\text{-}BdiPT = N\text{-benzoyl-}N',N'\text{-diphenylthioureato}$ ,  $R = \text{phenyl}$  or  $\text{cyclohexyl}$ ) was well-defined and led primarily to the 'direct' formation of the  $\text{Rh}^{\text{III}}$ -acyl species,  $[\text{Rh}(S,O\text{-}BdiPT)(\text{COMe})(\text{I})(\text{PR}^1\text{R}^2\text{R}^3)]$ , via the  $\text{Rh}^{\text{III}}$ -alkyl intermediate,  $[\text{Rh}(S,O\text{-}BdiPT)(\text{Me})(\text{CO})(\text{I})(\text{PR}^1\text{R}^2\text{R}^3)]$ , which was only observed in small quantities. This was manifested in a fast equilibrium for the oxidative addition/reductive elimination which lies to the left side, coupled with a slower, rate-determining migratory insertion step. The reason for this was concluded to be in the steric effect exerted by primarily the  $S,O\text{-}BdiPT$  ligand and was nicely supported by the solid state data.

The reaction rate for the different complexes increased in the order of  $[\text{Rh}(S,O\text{-}BdiPT)(\text{CO})(\text{PPhCy}_2)] < [\text{Rh}(S,O\text{-}BdiPT)(\text{CO})(\text{PCy}_3)] < [\text{Rh}(S,O\text{-}BdiPT)(\text{CO})(\text{PPh}_3)] < [\text{Rh}(S,O\text{-}BdiPT)(\text{CO})(\text{PPh}_2\text{Cy})]$ .

However, in the case of the  $[\text{Rh}(N,O\text{-}ox)(\text{CO})(\text{PR}^1\text{R}^2\text{R}^3)]$  complexes [small  $N,O\text{-}ox$  steric effect], the formation of the  $\text{Rh}^{\text{III}}$ -alkyl species as intermediate was well defined and significant amounts were observed.

The exact same order with respect to the  $\text{PR}_3$  ligand was observed within the  $[\text{Rh}(N,O\text{-}ox)(\text{CO})(\text{PR}^1\text{R}^2\text{R}^3)]$  complexes, although the second order forward rate constants for the  $N,O\text{-}ox$  complexes were approximately one order-of-magnitude progressively larger than for the corresponding  $S,O\text{-}BdiPT$  complexes. This order of reactivity was concluded to be the result of a combined effect of the steric (as primarily manifested in the  $X\text{-Rh-O}$  bite angles) and electronic properties of the ligands.

In both the  $S,O\text{-}BdiPT$  and  $N,O\text{-}ox$  ligand systems an associative activation is inferred from the large negative  $\Delta S^\ddagger$  values. Moreover, the relative reactivity of  $\text{Rh}^{\text{I}}\text{-}X,O\text{-}Bid$  complexes, where  $X=O, S$  or  $N$ , follows a surprising similar *reactivity relationship* when stepwise varying the  $\text{PPh}_3, \text{PPh}_2\text{Cy}, \text{PPhCy}_2$  and  $\text{PCy}_3$  tertiary phosphine ligands, suggesting a clear systematic behavior by the  $\text{PR}_3$  ligands, independent of the  $X,O\text{-}Bid$  ligand at the  $\text{Rh}(\text{I})$  metal centre.

## Experimental section

**General Procedures and Instrumentation.** NMR spectroscopic data was acquired on a Bruker Advance II 600 MHz spectrometer.  $^1\text{H}$  NMR data are listed in the order: chemical shift ( $\delta$ , reported in ppm and

referenced to the residual solvent peak of DMSO-d<sub>6</sub> [ $\delta$  = 2.50 ppm] or CD<sub>2</sub>Cl<sub>2</sub> [ $\delta$  = 5.33 ppm]), multiplicity, number of protons, assignment, coupling constant ( $J$ , in Hz). Proton decoupling experiments were used to assist in the assignment of proton signals. Proton decoupled <sup>13</sup>C NMR data are listed in the order: chemical shift ( $\delta$ , reported in ppm and referenced to the residual solvent peak of DMSO-d<sub>6</sub> [ $\delta$  = 39.5 ppm] or CD<sub>2</sub>Cl<sub>2</sub> [ $\delta$  = 77.0 ppm]), multiplicity, number of carbons, assignment, coupling constant ( $J$ , in Hz) where appropriate. HMQC experiments were performed to assist in the allocation of signals. Proton and carbon decoupled <sup>31</sup>P NMR data are listed in the order: chemical shift ( $\delta$ , reported in ppm and referenced to triphenylphosphine oxide [ $\delta$  = 29.9 ppm]), multiplicity, number of phosphorus atoms, coupling constant ( $J$ , in Hertz) where appropriate. FT-IR spectra were recorded on a Bruker Tensor 27 spectrophotometer in the range of 3000-600 cm<sup>-1</sup> via the ATR.

**Synthesis.** *N*-benzoyl-*N',N'*-(diphenyl)thiourea (*S,O*-BdiPT)H (**1**) was synthesized according to a modified literature procedure:<sup>9</sup> ammonium thiocyanate (1.31 g, 0.017 mol) was dissolved in hot acetone (10 mL). Benzoyl chloride (2 mL, 0.017 mol) was then added drop-wise upon which the reaction mixture changed to a milky, light yellow solution. The by-product ammonium chloride precipitated as the reaction proceeded. After 20 minutes the reaction mixture was filtered, the filtrate was collected and heated. Diphenylamine (0.017 mol) was then slowly added to the solution, after which the reaction mixture was allowed to stir for 30 minutes. The thiourea ligand was then precipitated with distilled water, collected by filtration and washed with a few portions of water. The product was then recrystallized from ethanol. The product was obtained as a white solid in a yield of 98%. <sup>1</sup>H NMR (600 MHz, DMSO-d<sub>6</sub>, 25 °C):  $\delta$  11.19 (s, 1H, CONHCS), 7.63 (d, 2H, *o*-benzoyl-H,  $J_{H-H}$  = 8.4 Hz), 7.51 (t, 1H, *p*-benzoyl-H,  $J_{H-H}$  = 7.3 Hz), 7.39 (t, 2H, *m*-benzoyl-H,  $J_{H-H}$  = 7.8 Hz), 7.36- 7.35 (m, 4H, *m*-Ph-H), 7.30-7.28 (m, 4H, *o*-Ph-H), 7.23- 7.21 (m, 2H, *p*-Ph-H). <sup>13</sup>C {<sup>1</sup>H} NMR (151 MHz, DMSO-d<sub>6</sub>, 25 °C):  $\delta$  184.5 (s, 1C, thiourea), 167.3 (s, 1C, amide), 145.6 (s, 2C, *i*-Ph-C), 132.7 (s, 1C, *i*-benzoyl-C), 132.3 (s, 1C, *p*-benzoyl-C), 129.1 (s, 4C, *o*-Ph-CH), 128.2 (s, 2C, *o*-benzoyl-CH), 128.1 (s, 2C, *m*-benzoyl-CH), 127.0 (s, 2C, *p*-Ph-CH), 126.8 (s, 4C, *m*-Ph-CH). IR  $\nu_{max}$  ATR/cm<sup>-1</sup>: 3215-3125 (broad, N-H); 1691 (C=O); 1504-1447 (broad, phenyl rings); 1354 (aromatic amide C-N); 1255 (C=S); 1183, 1160 and 1072 (C-N). Elemental analysis (%): Found C, 72.1; H, 5.0; N, 8.35. Calculated for C<sub>20</sub>H<sub>16</sub>N<sub>2</sub>SO: C, 72.3; H, 4.85; N, 8.4.

**General synthesis of rhodium(I) *S,O*-BdiPT carbonyl phosphine complexes.** RhCl<sub>3</sub>.xH<sub>2</sub>O (125.9 mg, 0.478 mmol) was heated in DMF (5 mL) at 180 °C to produce tetracarbonyl-dichloro-dirhodium(I).<sup>10</sup> *N*-benzoyl-*N',N'*-(diphenyl)thiourea (*S,O*-BdiPTH) 1 eq, 0.478 mmol) was slowly added to the cooled solution, which caused the colour of the solution to change from yellow to a bright orange, indicating the

formation of the expected  $[\text{Rh}(\text{S},\text{O}-(\text{S},\text{O}-\text{BdiPT})(\text{CO})_2)]$  complex. After about 10 minutes the complex was precipitated as a bright orange solid by the addition of ice water. After centrifugation the complex was taken up in diethyl ether and carefully removed from the excess water. Phosphine ligand (1 eq, 0.478 mmol) was added slowly to the ether solution. After a short time the desired complex  $[\text{Rh}(\text{S},\text{O}-\text{BdiPT})(\text{CO})(\text{PR}^1\text{R}^2\text{R}^3)]$  precipitated from solution as a yellow microcrystalline solid. The product was filtered and washed with several portions of ether. Crystals suitable for X-ray analysis were obtained by redissolving the complex in dichloromethane and layering the solution with hexane.

*Rhodium(I) (S,O-(N-benzoyl-N',N'-diphenylthiourea) carbonyl triphenylphosphine*  $[\text{Rh}(\text{S},\text{O}-\text{BdiPT})(\text{CO})(\text{PPh}_3)]$  (**2**). The product was obtained as a yellow microcrystalline solid in a yield of 65%.  $^1\text{H}\{^31\text{P}\}$  NMR (600 MHz,  $\text{CD}_2\text{Cl}_2$ , 25 °C):  $\delta$  7.69-7.66 (m, 5H, *o*-benzoyl-H, *p*-PPh-H), 7.47-7.38 (m, 16H, *m*-benzoyl-H, *o*-NPh-H, *m*-NPh-H, *o*-PPh-H), 7.33-7.31 (m, 2H, *p*-NPh-H), 7.19 (tt, 1H, *p*-benzoyl-H,  $^3J_{\text{H-H}} = 7.5$  Hz,  $^4J_{\text{H-H}} = 1.5$  Hz) 6.89-6.82 (m, 6H, *m*-PPh-H).  $^{13}\text{C}\{^1\text{H}\}$  NMR (151 MHz,  $\text{CD}_2\text{Cl}_2$ , 25 °C):  $\delta$  191.1 (dd, 1C, carbonyl,  $^1J_{\text{Rh-C}} = 74.1$  Hz,  $^2J_{\text{C-P}} = 21.1$  Hz), 178.9 (s, 1C, thiourea), 170.7 (s, 1C, amide), 145.8 (s, 2C, *i*-NPh-C), 137.5 (s, 1C, *i*-benzoyl-C), 134.9 (d, 6C, *o*-PPh-CH,  $^3J_{\text{C-P}} = 12.1$  Hz), 133.4 (d, 3C, *i*-PPh-C,  $J_{\text{C-P}} = 44.7$  Hz), 131.7 (s, 1C, *p*-benzoyl-CH), 130.9 (s, 3C, *p*-PPh-CH), 130.0 (s, 2C, *o*-benzoyl-CH), 129.8 (s, 4C, *o*-NPh-CH), 129.0 (s, 4C, *m*-NPh-CH), 129.0 (s, 6C, *m*-PPh-CH), 128.0 (s, 2C, *m*-benzoyl-CH), 127.7 (s, 2C, *p*-NPh-CH).  $^{31}\text{P}\{^1\text{H}, ^{13}\text{C}\}$  NMR (121 MHz,  $\text{CD}_2\text{Cl}_2$ , 25 °C):  $\delta$  38.2 (d,  $^1J_{\text{Rh-P}} = 152.3$  Hz). IR  $\nu_{\text{max}}$   $\text{CH}_2\text{Cl}_2/\text{cm}^{-1}$ : 1979 (CO),  $\nu_{\text{max}}$  ATR/ $\text{cm}^{-1}$ : 1963 (CO). Elemental analysis (%): Found C, 64.6; H, 4.1; N, 3.95. Calculated for  $\text{RhC}_{39}\text{H}_{30}\text{N}_2\text{SO}_2\text{P}$ : C, 64.6; H, 4.2; N, 3.9.

*Rhodium(I) (S,O-(N-benzoyl-N',N'-diphenylthiourea) carbonyl cyclohexyldiphenylphosphine*  $[\text{Rh}(\text{S},\text{O}-\text{BdiPT})(\text{CO})(\text{PPh}_2\text{Cy})]$  (**3**). The product was obtained as a yellow crystalline solid in a yield of 60%.  $^1\text{H}\{^31\text{P}\}$  NMR (600 MHz,  $\text{CD}_2\text{Cl}_2$ , 25 °C):  $\delta$  7.83-7.81 (m, 4H, *o*-benzoyl-H, *p*-PPh-H), 7.45-7.44 (m, 8H, *o*-NPh-H, *m*-NPh-H), 7.43-7.38 (m, 6H, *m*-benzoyl-H, *o*-PPh-H), 7.33 (m, 2H, *p*-NPh-H), 7.25-7.22 (m, 1H, *p*-benzoyl-H), 6.95-6.94 (m, 4H, *m*-PPh-H), 2.75-2.73 (m, 1H, 1-Cy-H), 2.11 and 1.80 (m, 4H, 2-Cy-H, 6-Cy-H), 1.73 and 1.19 (m, 2H, 4-Cy-H), 1.45-1.41 (m, 4H, 3-Cy-H, 5-Cy-H).  $^{13}\text{C}\{^1\text{H}\}$  NMR (151 MHz,  $\text{CD}_2\text{Cl}_2$ , 25 °C):  $\delta$  191.4 (dd, 1C, carbonyl,  $^1J_{\text{Rh-C}} = 73.8$  Hz,  $^2J_{\text{C-P}} = 21.3$  Hz), 179.2 (s, 1C, thiourea), 170.6 (s, 1C, amide), 146.9 (s, 2C, *i*-NPh-C), 137.7 (s, 1C, *i*-benzoyl-C), 134.2 (d, 4C, *o*-PPh-CH,  $J_{\text{C-P}} = 10.6$  Hz), 132.6 (d, 2C, *i*-PPh-C,  $J_{\text{C-P}} = 39.9$  Hz), 131.6 (s, 1C, *p*-benzoyl-CH), 130.5 (s, 2C, *p*-PPh-CH), 130.0 (s, 2C, *o*-benzoyl-CH), 129.7 (s, 4C, *o*-NPh-CH), 129.0 (s, 4C, *m*-NPh-CH), 128.9 (s, 4C, *m*-PPh-CH), 128.0 (s, 2C, *m*-benzoyl-CH), 127.7 (s, 2C, *p*-NPh-CH), 35.9 (d, 1C, 1-Cy-CH,  $^3J_{\text{C-P}} = 27.6$  Hz), 29.4 (s, 2C, 3-Cy-CH<sub>2</sub>, 5-Cy-CH<sub>2</sub>), 27.5 (d, 2C, 2-Cy-CH<sub>2</sub>, 6-Cy-CH<sub>2</sub>,  $J_{\text{C-P}} = 12.7$

Hz), 26.7 (s, 1C, 4-Cy-CH<sub>2</sub>). <sup>31</sup>P{<sup>1</sup>H, <sup>13</sup>C} NMR (121 MHz, CD<sub>2</sub>Cl<sub>2</sub>, 25 °C): δ 45.3 (d, <sup>1</sup>J<sub>Rh-P</sub> = 149.4 Hz). IR ν<sub>max</sub> CH<sub>2</sub>Cl<sub>2</sub>/cm<sup>-1</sup>: 1972 (CO), ν<sub>max</sub> ATR/cm<sup>-1</sup>: 1966 (CO). Elemental analysis (%): Found C, 64.1; H, 5.0; N, 4.1. Calculated for RhC<sub>39</sub>H<sub>36</sub>N<sub>2</sub>SO<sub>2</sub>P: C, 64.1; H, 5.0; N, 3.8.

*Rhodium(I) (S,O-(N-benzoyl-N',N'-diphenylthioureato) carbonyl dicyclohexylphenylphosphine*

*[Rh(S,O-BdiPT)(CO)(PPhCy<sub>2</sub>)] (4)*. The product was obtained as a yellow crystalline solid in a yield of 57%. <sup>1</sup>H{<sup>31</sup>P} NMR (600 MHz, CD<sub>2</sub>Cl<sub>2</sub>, 25 °C): δ 7.80-7.77 (m, 3H, *o*-benzoyl-H, *p*-PPh-H), 7.50-7.47 (m, 8H, *o*-NPh-H, *m*-NPh-H), 7.40-7.36 (m, 4H, *m*-benzoyl-H, *o*-PPh-H), 7.35 (m, 2H, *p*-NPh-H), 7.24-7.22 (m, 1H, *p*-benzoyl-H), 6.92-6.90 (m, 2H, *m*-PPh-H), 2.69-2.67 (m, 2H, 1-Cy-H), 2.15 and 1.84 (m, 8H, 2-Cy-H, 6-Cy-H), 1.70 and 1.21 (m, 4H, 4-Cy-H), 1.47-1.43 (m, 8H, 3-Cy-H, 5-Cy-H). <sup>13</sup>C{<sup>1</sup>H} NMR (151 MHz, CD<sub>2</sub>Cl<sub>2</sub>, 25 °C): δ 191.0 (dd, 1C, carbonyl, <sup>1</sup>J<sub>Rh-C</sub> = 74.2 Hz, <sup>2</sup>J<sub>C-P</sub> = 21.4 Hz), 179.0 (s, 1C, thiourea), 169.9 (s, 1C, amide), 145.40 (s, 2C, *i*-NPh-C), 137.4 (s, 1C, *i*-benzoyl-C), 135.1 (d, 2C, *o*-PPh-CH, J<sub>C-P</sub> = 7.8 Hz), 131.0 (s, 1C, *p*-benzoyl-CH), 130.1 (s, 1C, *p*-PPh-CH), 129.3 (s, 2C, *o*-benzoyl-CH), 129.1 (s, 4C, *o*-NPh-CH), 128.5 (broad s, 1C, *i*-PPh-C), 127.8 (s, 4C, *m*-NPh-CH), 127.7 (s, 2C, *m*-PPh-CH), 127.4 (s, 2C, *m*-benzoyl-CH), 127.0 (s, 2C, *p*-NPh-CH), 32.2 (d, 2C, 1-PCy-CH, <sup>3</sup>J<sub>C-P</sub> = 20.5 Hz), 28.6, 27.8 (s, 4C, 3-PCy-CH<sub>2</sub>, 5-PCy-CH<sub>2</sub>), 26.9, 26.7 (s, 4C, 2-PCy-CH<sub>2</sub>, 6-PCy-CH<sub>2</sub>), 26.1 (s, 2C, 4-PCy-CH<sub>2</sub>). <sup>31</sup>P{<sup>1</sup>H, <sup>13</sup>C} NMR (121 MHz, CD<sub>2</sub>Cl<sub>2</sub>, 25 °C): δ 49.5 (d, <sup>1</sup>J<sub>Rh-P</sub> = 149.0 Hz). IR ν<sub>max</sub> CH<sub>2</sub>Cl<sub>2</sub>/cm<sup>-1</sup>: 1969 (CO), ν<sub>max</sub> ATR/cm<sup>-1</sup>: 1961 (CO). Elemental analysis (%): Found C, 63.7; H, 5.8; N, 4.0. Calculated for RhC<sub>39</sub>H<sub>42</sub>N<sub>2</sub>SO<sub>2</sub>P: C, 63.6; H, 5.8; N, 3.8.

*Rhodium(I) (S,O-(N-benzoyl-N',N'-diphenylthioureato) carbonyl tricyclohexylphosphine [Rh(S,O-BdiPT)(CO)(PCy<sub>3</sub>)] (5)*. The product was obtained as a yellow crystalline solid in a yield of 63%.

<sup>1</sup>H{<sup>31</sup>P} NMR (600 MHz, CD<sub>2</sub>Cl<sub>2</sub>, 25 °C): δ 7.68 (dd, 2H, *o*-benzoyl-H, J<sub>H-H</sub> = 8.4 Hz, J<sub>H-H</sub> = 1.5 Hz), 7.44-7.43 (m, 8H, *o*-Ph-H, *m*-Ph-H), 7.37 (tt, 1H, *p*-benzoyl-H, <sup>3</sup>J<sub>H-H</sub> = 7.4 Hz, <sup>4</sup>J<sub>H-H</sub> = 1.2 Hz), 7.33-7.31 (m, 2H, *p*-Ph-H), 7.21 (t, 2H, *m*-benzoyl-H, <sup>3</sup>J<sub>H-H</sub> = 7.8 Hz), 2.33-2.27 (m, 3H, 1-Cy-H), 2.05 and 1.80 (d, 12H, 2-Cy-H, 6-Cy-H, <sup>3</sup>J<sub>H-H</sub> = 12.0 Hz), 1.65 and 1.25 (m, 18H, 3-Cy-H, 4-Cy-H, 5-Cy-H). <sup>13</sup>C{<sup>1</sup>H} NMR (151 MHz, CD<sub>2</sub>Cl<sub>2</sub>, 25 °C): δ 191.9 (dd, 1C, carbonyl, <sup>1</sup>J<sub>Rh-C</sub> = 75.2 Hz, <sup>2</sup>J<sub>C-P</sub> = 20.7 Hz), 179.8 (s, 1C, thiourea), 171.0 (s, 1C, amide), 146.0 (s, 2C, *i*-Ph-C), 138.7 (s, 1C, *i*-benzoyl-C), 131.7 (s, 1C, *p*-benzoyl-CH), 130.1 (s, 2C, *o*-benzoyl-CH), 129.7 (s, 4C, *o*-Ph-CH), 129.1 (s, 4C, *m*-Ph-CH), 128.2 (s, 2C, *m*-benzoyl-CH), 127.6 (s, 2C, *p*-Ph-CH), 34.2 (d, 3C, 1-Cy-CH, <sup>2</sup>J<sub>C-P</sub> = 21.1 Hz), 30.6 (s, 6C, 3-Cy-CH<sub>2</sub>, 5-Cy-CH<sub>2</sub>), 28.3 (d, 6C, 2-Cy-CH<sub>2</sub>, 6-Cy-CH<sub>2</sub>, <sup>3</sup>J<sub>C-P</sub> = 10.7 Hz), 27.1 (s, 3C, 4-Cy-CH<sub>2</sub>). <sup>31</sup>P{<sup>1</sup>H, <sup>13</sup>C} NMR (121 MHz, CD<sub>2</sub>Cl<sub>2</sub>, 25 °C): δ 49.9 (d, <sup>1</sup>J<sub>Rh-P</sub> = 145.6 Hz). IR ν<sub>max</sub> CH<sub>2</sub>Cl<sub>2</sub>/cm<sup>-1</sup>: 1963 (CO), ν<sub>max</sub> ATR/cm<sup>-1</sup>: 1952 (CO). Elemental analysis (%): Found C, 62.7; H, 6.55; N, 3.9. Calculated for RhC<sub>39</sub>H<sub>48</sub>N<sub>2</sub>SO<sub>2</sub>P: C, 63.1; H, 6.5; N, 3.8.

*Dicarbonyl(oxinato)rhodium(I)*,  $[Rh(N,O-ox)(CO)_2]$ , (**6**). The complex  $[Rh(N,O-ox)(CO)_2]$  was prepared as reported in literature<sup>8,11</sup> by dissolving  $[Rh_2CO_4Cl_2]$  (100 mg, 0.257 mmol) in DMF (10 ml) and by the drop wise addition of 8-hydroxyquinoline (82.05 mg, 0.565 mmol) in DMF (5 ml) to the stirring reaction mixture. The product was obtained as a brown precipitate by addition of ice water, collected by filtration and washed with water. (Yield: 74.7 mg, 94 %). <sup>1</sup>H NMR (300 MHz, CDCl<sub>3</sub>, 25 °C): 8.653 (d, 1H), 8.374 (d, 1H), 7.502 (m, 2H), 7.134 (m, 2H). IR KBr:  $\nu_{CO} = 2075$  and  $2005\text{ cm}^{-1}$ .

*Carbonyl(triphenylphosphine)(oxinato)rhodium(I)*,  $[Rh(N,O-ox)(CO)(PPh_3)]$ , (**7**). The complex  $[Rh(N,O-ox)(CO)(PPh_3)]$  was prepared as reported in literature<sup>8,11</sup> by drop-wise addition of PPh<sub>3</sub> (30 mg, 0.114 mmol) in acetone (10ml) to a stirring solution of  $[Rh(N,O-ox)(CO)_2]$  (31 mg, 0.103 mmol) in acetone (40 ml). Solvent evaporation to dryness yielded the product as yellow crystals. (Yield: 51 mg, 93 %). <sup>1</sup>H NMR (300 MHz, CDCl<sub>3</sub>, 25 °C): 8.771 (d, 1H), 8.248 (d, 1H), 7.806 – 7.646 (m, 8H), 7.482 – 7.373 (m, 9H), 6.963 (d, 1H), 6.88 (d, 1H). <sup>1</sup>J(Rh-P) = 164 Hz. IR KBr:  $\nu_{CO} = 1965\text{ cm}^{-1}$ .  $\lambda_{max}(\text{acetone}) = 420\text{ nm}$  ( $\epsilon = 3351$ ).

*Carbonyl(cyclohexyldiphenylphosphine)(oxinato)rhodium(I)*,  $[Rh(N,O-ox)(CO)(PPh_2Cy)]$ , (**8**). The complex  $[Rh(N,O-ox)(CO)(PPh_2Cy)]$  was prepared according to the procedure described for synthesis of  $[Rh(N,O-ox)(CO)(PPh_3)]$ . By addition of PPh<sub>2</sub>Cy (17.6 mg, 0.064 mmol) to  $[Rh(N,O-ox)(CO)_2]$  (18 mg, 0.059 mmol), the product was obtained as a yellow crystalline solid. (Yield: 25 mg, 77 %). <sup>1</sup>H NMR (300 MHz, CDCl<sub>3</sub>, 25 °C): 8.717 (s, 1H), 8.225 (d, 1H), 7.866 – 7.417 (m, 12H), 6.918 (dd, 2H), 1.810 – 1.273 (m, 11H). <sup>1</sup>J(Rh-P) = 163 Hz. IR KBr:  $\nu_{CO} = 1959\text{ cm}^{-1}$ .  $\lambda_{max}(\text{acetone}) = 420\text{ nm}$  ( $\epsilon = 4512$ ).

*Carbonyl(dicyclohexylphenylphosphine)(oxinato)rhodium(I)*,  $[Rh(N,O-ox)(CO)(PPhCy_2)]$ , (**9**). The complex  $[Rh(N,O-ox)(CO)(PPhCy_2)]$  (**9**) was synthesised according to the procedure described for synthesis of  $[Rh(N,O-ox)(CO)(PPh_3)]$ . By addition of PPhCy<sub>2</sub> (18 mg, 0.069 mmol) to  $[Rh(N,O-ox)(CO)_2]$  (19 mg, 0.062 mmol), the product was obtained as a yellow solid. (Yield: 28 mg, 82 %). <sup>1</sup>H NMR (300 MHz, CDCl<sub>3</sub>, 25 °C): 8.819 (s, 1H), 8.612 (d, 1H), 7.924 – 7.868 (m, 2H), 7.501 – 7.459 (m, 5H), 6.784 (d, 1H), 1.827 – 1.728 (M.14H), 1.469 – 1.334 (m, 8H). <sup>1</sup>J(Rh-P) = 161 Hz. IR KBr:  $\nu_{CO} = 1952\text{ cm}^{-1}$ .  $\lambda_{max}(\text{acetone}) = 420\text{ nm}$  ( $\epsilon = 5430$ ).

*Carbonyl(tricyclohexylphosphine)(oxinato)rhodium(I)*,  $[Rh(N,O-ox)(CO)(PCy_3)]$ , (**10**). The complex  $[Rh(N,O-ox)(CO)(PCy_3)]$  (**10**) was prepared according to the procedure described for synthesis of  $[Rh(N,O-ox)(CO)(PPh_3)]$ . By addition of PCy<sub>3</sub> (20 mg, 0.072 mmol) to  $[Rh(N,O-ox)(CO)_2]$  (19 mg, 0.059 mmol), the product was obtained as a yellow crystalline solid. (Yield: 20 mg, 62 %). <sup>1</sup>H NMR (300 MHz, CDCl<sub>3</sub>, 25 °C): 8.716 (s, 1H), 8.187 (d, 1H), 7.396 – 7.290 (m, 2H), 6.855 (dd, 2H), 2.163 – 1.311 (m, 33H). <sup>1</sup>J(Rh-P) = 156 Hz. IR KBr:  $\nu_{CO} = 1946\text{ cm}^{-1}$ .  $\lambda_{max}(\text{acetone}) = 420\text{ nm}$  ( $\epsilon = 4224$ ).

**X-ray Data Collection, Reduction, and Refinement.** Initial unit cell and data collections were performed on a Bruker X8 Apex II 4K Kappa CCD diffractometer using graphite monochromated Mo K $\alpha$  radiation ( $\lambda = 0.70926 \text{ \AA}$ ) with  $\omega$ - and  $\phi$ -scans at 100(2) K as well as the Apex2 software package.<sup>17</sup> The optimum measurement method to collect more than a hemisphere of reciprocal space was predicted by COSMO.<sup>18</sup> Frame integration and data reductions were performed using the SAINT-Plus and XPREP software packages,<sup>16,19</sup> and a multi-scan absorption correction was performed on the data using SADABS. The structures were solved by the direct methods package SIR97,<sup>20</sup> and refinement using the WinGX software package<sup>21</sup> incorporating SHELXL.<sup>22</sup> All non-hydrogen atoms were refined anisotropically. All H-atoms were positioned geometrically and refined using a riding model with fixed C-H distances of 0.95  $\text{\AA}$  (CH) [ $U_{\text{iso}}(\text{H}) = 1.2U_{\text{eq}}$ ] for aromatic H-atoms and 0.98  $\text{\AA}$  (CH) [ $U_{\text{iso}}(\text{H}) = 1.2U_{\text{eq}}$ ] for methyl H-atoms as well as fixed N-H distances of 0.88  $\text{\AA}$  (NH) [ $U_{\text{iso}}(\text{H}) = 1.2U_{\text{eq}}$ ]. Molecular diagrams were drawn using the Mercury package<sup>23</sup> with a 30% thermal envelope probability for non-hydrogen atoms.

**Kinetic Experiments.** All kinetic experiments were carried out in air and all solvents were pre-dried over aluminium oxide and distilled.  $^1\text{H}$ ,  $^{13}\text{C}$  and  $^{31}\text{P}$  NMR spectra were recorded on either 300 MHz and 600 MHz Bruker spectrometers. The  $^{13}\text{C}$ ,  $^{31}\text{P}$  and  $^1\text{H}$  FT-NMR spectra were recorded at 150.96, 243.0 and 600.28 MHz respectively on a Bruker AXS 600 MHz at 25 $^\circ\text{C}$  chemical shifts are reported in ppm.  $^{13}\text{C}$  NMR spectra were calibrated relative to the  $^{13}\text{C}$  resonances for  $\text{CD}_2\text{Cl}_2$  and to tetramethylsilane (TMS) and 80%  $\text{H}_3\text{PO}_4$  for  $^1\text{H}$  and  $^{31}\text{P}$  respectively. Alternatively, the  $^1\text{H}$  (300MHz) and  $^{31}\text{P}$  (121.495 MHz) NMR spectra were also recorded on a BRUKER advance DPX 300 spectrometer at 25  $^\circ\text{C}$  in  $\text{CD}_2\text{Cl}_2$  solution. Chemical shifts were referenced with respect to tetramethylsilane (TMS) and 80%  $\text{H}_3\text{PO}_4$  for  $^1\text{H}$  and  $^{31}\text{P}$  respectively.  $^{31}\text{P}$  NMR were recorded with the default setting of 1-H decoupling using the WALTZ16 method, typical 64 or 128 scans, a sweep width of 400.5 ppm (48661.8 Hz) a delay time (D1) of 2 sec. and 64 K Points.

FT-IR spectra were recorded as liquid samples in dry organic solvents (toluene or dichloromethane) in a NaCl cell on a Bruker Tensor 27 spectrometer in the range of 2350-1600  $\text{cm}^{-1}$ , equipped with a temperature cell regulator accurate within 0.3  $^\circ\text{C}$ . UV/Vis absorbance spectra were collected on a Varian Cary 50 Conc spectrophotometer in a  $1.000 \pm 0.001 \text{ cm}$  quartz cuvette, which was equipped with a

temperature cell regulator accurate within 0.1 °C. Kinetic data was analyzed with the Scientist software package.<sup>24</sup>

### **Associated content**

### **Supporting Information**

X-ray crystallographic data in CIF format and has been deposited at the Cambridge Crystallographic Data Centre for **2**, **3**, **5** and **10**, as CCDC 1827388-1827391. This information is available free of charge via the Internet at the Cambridge Crystallographic Data Centre; <http://www.ccdc.cam.ac.uk/>. Additional figures and kinetic are included in the Supplementary Information deposited at the Journal's editorial office.

Author information

### **Corresponding Author**

roodta@ufs.ac.za

Notes

The authors declare no competing financial interest.

### **Acknowledgment**

The authors thank SASOL, the South African NRF and THRIP, the Swiss National Science Foundation, and the University of the Free State Research Fund and the Materials and Nanosciences Research Cluster for financial support. The views expressed do not necessarily represent that of the NRF.

## References

---

1. P. W. N. M. van Leeuwen, *Homogeneous Catalysis: Understanding the Art*, Springer, **2004**; G. Rothenberg, *Catalysis*, 1st ed., Wiley-VCH Verlag GmbH & Co., Weinheim, **2008**.
2. Maitlis, P. M.; Haynes, A.; Sunley, G. J.; Howard, M. J. *J. Chem. Soc. Dalton Trans.* **1996**, 2187.
3. (a) Basson, S. S.; Leipoldt, J. G.; Roodt, A.; Venter, J. A. *Inorg. Chim. Acta*, **1987**, *128*, 31; (b) Brink, A.; Roodt, A.; Steyl, G.; Visser, H. G. *Dalton Trans.* **2010**, 5572; (c) Conradie, J.; Lamprecht, G.J.; Otto, S.; Swarts, J.C. *Inorg. Chim. Acta* **2002**, *328*, 191; (d) Erasmus, J.J.C.; Swarts, J.C. *Polyhedron* **1998**, *17*, 2447; Conradie, J.; Swarts, J. C. *Organometallics* **2009**, *28*, 1018; (e) Conradie, M. M.; Conradie, J. *Inorg. Chim. Acta* **2008**, *361*, 208; (f) Stuurman, N.F.; Conradie, J. *J. Organomet. Chem.* **2009**, *694*, 259.
4. Conradie, M.M.; van Rooyen, P.H.; Pretorius, C.; Roodt, A.; Conradie, J. *J. Mol. Struct.* **2017**, *1144*, 280.
5. Cheng, C.-H.; Spivack, B. D.; Eisenberg, R. *J. Am. Chem. Soc.* **1977**, *99*, 3003.
6. (a) Steyn, G. J. J.; Roodt, A.; Leipoldt, J. G. *Rhodium Express*, **1993**, *1*, 25; (b) Gonsalvi, L.; Adams, H.; Sunley, G. J.; Ditzel, E.; Haynes, A. *J. Am. Chem. Soc.*, **2002**, *124*, 13597.
7. (a) Venter, J. A.; Leipoldt, J. G.; van Eldik, R. *Inorg. Chem.* **1991**, *30*, 2207; (b) Leipoldt, J. G.; Basson, S. S.; Botha, L. J. *Inorg. Chim. Acta*, **1990**, *168*, 215; (c) Warsink, S.; Roodt, A.; Venter, J.A.; Kotze, P.D.R.; Otto, S. *Z. Kristallogr. NCS* **2013**, *228*, 335; (d) Warsink, S.; Roodt, A.; Venter, J.A.; Kotze, P.D.R.; Otto, S. *Z. Kristallogr. NCS* **2013**, *228*, 428; (e) Koch, K.R. *Coord. Chem. Rev.* **2001**, *245*, 121.
8. Van Aswegen, K.G.; Leipoldt, J.G.; Potgieter, I.M.; Roodt, A.; van Zyl G.J. *Trans. Met. Chem.* **1991**, *16*, 369.
9. Douglass, I. B.; Dains, F. B. *J. Am. Chem. Soc.*, **1934**, *56*, 719.
10. McCleverty, J. A.; Wilkinson, G. *Inorg. Synth.* **1990**, *28*, 84.
11. (a) Leipoldt, J. G.; Basson S. S.; Dennis, C.R. *Inorg. Chim. Acta*, **1981**, *50*, 121; (b) Janse van Rensburg, J.M.; Roodt, A.; Muller, A. *Acta Crystallogr., Sect.E: Struct. Rep. Online* **2006**, *62*, m1040.
12. (a) Leipoldt, J. G.; Basson, S. S.; Botha, L. J. *Inorg. Chim. Acta*, **1990**, *68*, 215; (b) Steyn, G. J. J.; Roodt, A.; Leipoldt, J. G. *Inorg. Chem.*, **1992**, *31*, 3477.
13. (a) Warsink, S.; Fessha, F. G.; Purcell, W.; Venter, J. A. *J. Organomet. Chem.* **2013**, *726*, 14; (b) Purcell, W.; Conradie, J.; Chiweshe, T.T.; Venter, J.A.; Twigge, L.; Coetzee, M.P. *J. Organomet. Chem.* **2013**, *745-6*, 439; (c) Erasmus, J.J.C.; Conradie, J. *Cent. Eur. J. Chem.* **2012**, *10*, 256; (d) Erasmus, J.J.C.; Conradie, M.M.; Conradie, J. *React. Kin. Mech. Cat.* **2012**, *B105*: 233; (e) Otto, S.; Roodt, A.; Conradie, M. M.; Conradie, J. *Inorg. Chim. Acta* **2008**, *361*, 2285; (f) Conradie, M. M.; Conradie, J. *Inorg. Chim. Acta* **2009**, *362*, 519; (g) Conradie, M. M.; Conradie, J. *S. Afr. J. Chem.* **2008**, *61*, 102.
14. (a) Roodt, A.; Otto, S.; Steyl, G. *Coord. Chem. Rev.* **2003**, *245*, 121; (b) Roodt, A.; Steyn, G. J.; Pandalai, S. G. *Res. Research Dev. Inorg. Chem.*, vol. 2, Transworld Research Network, Trivandrum, **2000**, 1; (c) Roodt, A., Visser, H.G., Brink, A., *Cryst. Revs.* **2011**, *17*, 241; (d) Cloete, N.; Visser, H.G.; Engelbrecht, I.; Overett, M.J.; Gabrielli, W.F.; Roodt, A. *Inorg. Chem.* **2013**, 2268.

15. Muller, A.; Otto, S.; Roodt, A. *Dalton Trans.* **2008**, 650-657.
16. Bunten, K. A.; Moreno, C.; Poë, A. J. *Dalton Trans.*, **2005**, 1416.
17. Bruker, *Apex2* (Version 1.0-27). Bruker AXS Inc., Madison, Wisconsin, USA, **2005**.
18. Bruker, *COSMO* (Version 1.48). Bruker AXS Inc., Madison, Wisconsin, USA, **2003**.
19. Bruker, *SAINTE-Plus* including *XPREP* (Version 7.12). Bruker AXS Inc., Madison, Wisconsin, USA, **2004**.
20. Altomare, A.; Burla, M. C.; Camalli, M.; Cascarano, G. L.; Giacovazzo, C.; Guagliardi, A.; Moliterni, A. G. G.; Polidori, G.; Spagna, R. *J. Appl. Cryst.* **1999**, 32, 115.
21. Farrugia, L. J., *J. Appl. Cryst.* **1999**, 32, 837.
22. (a) Sheldrick, G. M. *SHELXL97*; University of Göttingen, Germany, **1997**. (b) Sheldrick, G. M. *Acta Cryst.* **2008**, A64, 112-122.
23. Macrae, C. F.; Edgington, P. R.; McCabe, P.; Pidcock, E.; Shields, G. P.; Taylor, R.; Towler, M.; van de Streek, J. *J. Appl. Cryst.* **2006**, 39, 453.
24. Micromath, *Scientist for Windows* (Version 2.01), Micromath Inc., **1995**.